Argon Plasma-Induced Quantum Well Intermixing for Monolithic Photonic Integration

Xin Zhang and Jian-Jun He, *Senior Member, IEEE*

(Year I Paper)

***Abstract*—Models and formulations needed for the calculation of the optical properties of the diffused quantum wells are analyzed in this paper.**

***Index Terms*—Photonic integrated circuits (PICs), quantum well intermixing (QWI), polarization independence.**

I. Introduction

IN THE past decades, there have been a large number of studies of quantum well intermixing (QWI) with the aim to develop the technique for monolithic integration of optoelectronic devices and photonic integrated circuits (PICs) applications [1]. With this technique, it is possible to selectively modify the composition variation within a small region in a wafer. The emerged technology of QWI, such as ion-implantation induced disordering (IIID) [2], impurity-free vacancy disordering (IFVD) [3], sputtered silica-induced intermixing [4], photoabsorption-induced disordering (PAID) [5] and argon-plasma enhanced quantum well intermixing [6], have been utilized in wide application for PICs, such as the 40-Gb/s Widely Tunable Transceivers by UCSB [7].

In the meanwhile, theory works of QWI have been carried out which play an important role in understanding the mechanics and optimizing the performance of this technology. By far, there has been a widely accepted theory of QWI, which talks about the optical properties, including stimulated wavelength, optical absorption, and optical gain. The simulation results agree quite well with the experimentally measured values. I will talk about the simulation process in this paper. The interdiffusion mechanics of QWI, which is more complicated to understand, will be investigated in the next term.

This paper is organized as follows. The theoretical analysis of QWI are investigated in Section II. Fundamental experiments of QWI, including bandgap energy shift characteristics, waveguiding characteristics, electrical characteristics and carrier induced tuning characteristics are described in Section III. Some applications of QWI, including bandgap tuning of InP-based lasers and extended cavity laser, are presented and discussed in Section IV. Section V summarizes the main conclusions of this paper.

Manuscript received September 1, 2009; revised September 9, 2009.

X. Zhang is with the Center for Optical and Electromagnetic Research, State Key Laboratory of Modern Optical Instrumentation, Zhejiang University, Hangzhou 310058, China.

J.-J. He is with the Center for Optical and Electromagnetic Research, State Key Laboratory of Modern Optical Instrumentation, Zhejiang University, Hangzhou 310058, China. He is also with Lightip Technologies, Inc., Ottawa, ON K1K 4R8, Canada (e-mail: jj.he@lightip.com).

Digital Object Identifer 00.0001/LPT.2010.000001

II. Theoretical Analysis

A. Diffusion Model

Interdiffusion of atoms across the heterointerface alters the composition profile across the QW structure. Mathematical models are needed to describe and calculate the changes in the composition profile as a function of the duration of interdiffusion. In the section, we adopt the notation $A_xB_{1-x}C_yD_{1-y}$ to denote the chemical formula of a III-V semiconductor material, where A and B represent the Group III atoms, and C and D represent the Group V atoms respectively. After interdiffusion the mole fractions of Group III and V atoms are function of position along the direction of crystal growth (the z-direction) and are denoted by $w(z)$ and $v(z)$.

The diffusion process is usually described by the Fick's Second Law in the direction of crystal growth

$$\frac{\partial C}{\partial t} = D\frac{\partial^2 C}{\partial z^2} \tag{1}$$

where C denotes the concentration of the atoms and D is the diffusion coefficient. The diffusion coefficient of the atoms is usually assumed to be identical in the quantum well. The interdiffusion process is characterized by a diffusion length L_d, which is defined as $L_d = \sqrt{Dt}$, where D is the diffusion coefficient and t is the annealing time of the thermal processing. Consider a single $In_{wx}Ga_{1-wx}As_{wy}P_{1-wy}/In_{bx}Ga_{1-bx}As_{by}P_{1-by}$ quantum well, the composition profile of In and As in this QW after interdiffusion are given by

$$\begin{aligned} w(z) &= wx - \frac{bx-wx}{2} \\ &\quad \times\left[2 - \mathrm{erf}\left(\frac{L_z+2z}{4L_d^{III}}\right) - \mathrm{erf}\left(\frac{L_z-2z}{4L_d^{III}}\right)\right] \end{aligned} \tag{2}$$

$$\begin{aligned} v(z) &= wy - \frac{by-wy}{2} \\ &\quad \times\left[2 - \mathrm{erf}\left(\frac{L_z+2z}{4L_d^{V}}\right) - \mathrm{erf}\left(\frac{L_z-2z}{4L_d^{V}}\right)\right] \end{aligned} \tag{3}$$

In this case, interdiffusion can occur on both group III and V sublattices, which are characterized by their diffusion lengths L_d^{III} and L_d^V, respectively. The diffusion length ratio, i.e., $k = L_d^V/L_d^{III}$, depends on the details of interdiffusion process and is still an open question which requires further studies.

B. Band Structure

The optical properties of a non-square interdiffused quantum well depend on the band structure which can be found by using

some existing models, such as the envelop function approximation, pseudopotential method, the tight-binding model and the effective bond-orbital model. We use the envelop function approximation because of the computationally simplicity and enough accuracy for describing phenomena occurring on a length scale large compared with the unit cell of the crystal. The envelop function for the z-direction can be obtained by solving the Schrodinger-like equation shown below.

$$\frac{-h^2}{2}\frac{d}{dz}\frac{1}{m_{\perp}^{*}(z)}\frac{d\varphi(z)}{dz}+V(z)\varphi(z)=E\varphi(z) \quad (4)$$

where $m_{\perp}(z)$ is the effective mass of the conduction band or valence band. $V(z)$ is the position-dependent potential energy of the conduction band heavy hole valence band or light hole valence band, which can be determined by Equation 5-7, respectively. This differential equation is solved using the finite-difference method (FDM) with appropriate boundary conditions. Usually we consider the quantum well contained in a large box along the z-direction with the boundary condition $\varphi = 0$ at the boundaries of the box.

$$V_c(z)=Q_cEg(z)-(1-Q_c)S_{\perp}(z) \quad (5)$$

$$V_{HH}(z)=(1-Q_c)[Eg(z)-S_{\perp}(z)]+S_{\parallel}(z) \quad (6)$$

$$\begin{aligned}V_{LH}(z) &= (1-Q_c)[Eg(z)-S_{\perp}(z)]\\ &\quad +0.5[S_{\parallel}(z)+\Delta_0(z)]\\ &\quad -0.5\sqrt{9S_{\parallel}^2(z)-2S_{\parallel}^2(z)\Delta_0(z)+\Delta_0^2(z)}\end{aligned} \quad (7)$$

The calculation of the potential energy has take consideration the strain effect of the quantum well materials by Equation 8-11. All the material parameters for the numerical calculation can be obtained from Table I by [8].

$$S_{\perp}(z)=-2a_v(z)[1-\frac{C_{12}(z)}{C_{11}(z)}]\epsilon(z) \quad (8)$$

$$S_{\parallel}(z)=-b(z)[1+\frac{2C_{12}(z)}{C_{11}(z)}]\epsilon(z) \quad (9)$$

$$a_v(z)=-\frac{1}{3}[C_{11}(z)+2C_{12}(z)]\frac{dEg}{dp}(z) \quad (10)$$

$$\epsilon(z)=\frac{a_{InP}(z)-a(z)}{a(z)} \quad (11)$$

To show the validity of the theoretical model, I adopt the data by Nanyang Technology University with the same method of argon plasma-induced QWI [9]. The layer structure of samples used in the experiment is shown in Table II. Figure 1 shows the PL spectra of one InP cap sample before plasma exposure and after plasma exposure followed by several rapid thermal annealing (RTA) process. The result shows that after argon plasma exposure, both the blueshift and redshift of the bandgap can be obtained by controlling the temperature of RTA.

To interpret the above observations of bandgap modification, the wavelength shift of the interdiffused QW structure was calculated using my theoretical model. Figure 2 shows the calculated PL peak wavelength shift as a function of group III diffusion length under different k parameters. It can be seen that, in this QW structure, an observable redshift can be obtained only when k<0.63 roughly; i.e., the group III sublattice must interdiffuse about twice as fast as the group V sublattice.

TABLE II
THE LAYER STRUCTURE FOR THE UNDOPED INGAASP/INP SINGLE QUANTUM WELL

No.	Composition	Thickness(nm)	Layer
5	$In_{0.53}Ga_{0.47}As$	500	Buffer/cap
4	InP	500	Barrier/cap
3	$In_{0.71}Ga_{0.29}As_{0.61}P_{0.39}$	3.5	Well
2	InP	300	Barrier
1	InP	–	substrate

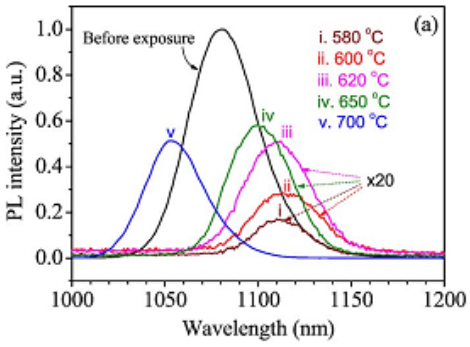

Fig. 1. PL spectra for one InP cap sample before plasma exposure and after plasma exposure followed by annealing at (i) 580°C, (ii) 600°C, (iii) 620°C, (iv) 650°C, (v) 700°C.

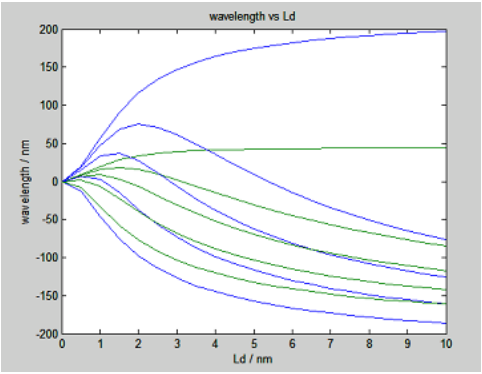

Fig. 2. The calculated wavelength shift of the ground state transition as a function of the group III diffusion length under different k parameters.

C. Optical Absorption

Subsection text here.

D. Quantum Confined Stark Effects

Subsection text here.

$$\frac{-h^2}{2}\frac{d}{dz}\frac{1}{m_{\perp}^{*}(z)}\frac{d\varphi(z)}{dz}+[V(z)+zeE]\varphi(z)=E\varphi(z) \quad (12)$$

TABLE I
MATERIAL PARAMETERS FOR INGAASP USED IN NUMERICAL CALCULATION AT ROOM TEMPERATURE (300K) OF QUANTUM WELLS STRUCTURES

Symbol	Parameter	$In_xGa_{1-x}As_yP_{1-y}$	Unit
$Q_c : Q_v$	Band offset splitting ratio	$0.6 : 0.4$	–
$E_g(z)$	Energy bandgap	$1.35 - 1.17y + 0.668(1-x) - 0.069y(1-x) + 0.18y^2$ $+0.03(1-x)y^2 + 0.758(1-x)^2 - 0.322y(1-x)^2$	eV
$\Delta_0(z)$	Spin-orbit splitting	$0.34(1-x)y + 0.43xy + 0.10(1-x)(1-y) + 0.10x(1-y)$	eV
m_e	Electron mass	$0.91095 \times 10{-}30$	kg
$m_c^*(z)$	Electron effective mass	$0.0632(1-x)y + 0.0213xy + 0.17(1-x)(1-y) + 0.077x(1-y)$	m_e
$m^*_{\perp HH}(z)$	Heavy hole effective mass perpendicular to QW layer	$0.5(1-x)y + 0.41xy + 0.54(1-x)(1-y) + 0.12x(1-y)$	m_e
$m^*_{\perp LH}(z)$	Light hole effective mass perpendicular to QW layer	$0.088(1-x)y + 0.024xy + 0.16(1-x)(1-y) + 0.12x(1-y)$	m_e
$m^*_{\parallel HH}(z)$	Heavy hole effective mass parallel to QW layer	$0.11(1-x)y + 0.031xy + 0.19(1-x)(1-y) + 0.15x(1-y)$	m_e
$m^*_{\parallel LH}(z)$	Light hole effective mass parallel to QW layer	$0.23(1-x)y + 0.082xy + 0.34(1-x)(1-y) + 0.29x(1-y)$	m_e
$a(z)$	Lattice constant	$0.56533(1-x)y + 0.60584xy + 0.54512(1-x)(1-y) + 0.58688x(1-y)$	nm
$C_{11}(z)$	Elastic stiffness constant	$11.8(1-x)y + 8.329xy + 14.12(1-x)(1-y) + 10.22x(1-y)$	$10^{11} dyn/cm^2$
$C_{12}(z)$	Elastic stiffness constant	$5.38(1-x)y + 4.526xy + 6.253(1-x)(1-y) + 5.76x(1-y)$	$10^{11} dyn/cm^2$
$dE_g/dP(z)$	Hydrostatic pressure coefficient	$11.5(1-x)y + 10.0xy + 11.0(1-x)(1-y) + 8.5x(1-y)$	$10^{-6} eV/bar$
$b(z)$	Shear deformation potential	$-1.7(1-x)y - 1.8xy - 1.5(1-x)(1-y) - 2.0x(1-y)$	eV

E. Optical Gain

Subsection text here.

$$g(\hbar\omega) = \frac{2m_r\omega}{n_{eff}c\varepsilon_0\pi\hbar^2 L_z}\sum_{n,m}\int_0^\infty dE_\parallel |e\cdot M_{cv}(E_\parallel)|^2 \times\frac{\frac{\hbar}{\pi\tau_{in}}}{(E_{en}-E_{hm}+E_\parallel-\hbar\omega)^2+(\frac{\hbar}{\pi\tau_{in}})^2} \times[f_c^n(E_\parallel)-f_v^m(E_\parallel)] \quad (13)$$

F. Refractive Index

Subsection text here.

$$\Delta n(\hbar\omega) = \frac{m_r}{n_{eff}c\varepsilon_0\pi\hbar^2 L_z}\sum_{n,m}\int_0^\infty dE_\parallel |e\cdot M_{cv}(E_\parallel)|^2 \times\frac{E_{en}-E_{hm}+E_\parallel-\hbar\omega}{(E_{en}-E_{hm}+E_\parallel-\hbar\omega)^2+(\frac{\hbar}{\pi\tau_{in}})^2} \times[f_c^n(E_\parallel)-f_v^m(E_\parallel)] \quad (14)$$

III. EXPERIMENTS

A. Parameters Affecting the Bandgap Energy Shifts in QWI

Parameters affecting the bandgap energy shifts in argon plasma-induced quantum well intermixing have previously been studied in detail elsewhere [10]. Inductively coupled plasma (ICP) parameters, RTA parameters and QW layer structure are three main factors affects the magnitude of bandgap energy shifts. In my experiments, ICP and RTA parameters were investigated.

The layer structure of the QW samples is shown in Table III. The plasma source generator used in the experiments was a Plasmalab System 100, which was built by Oxford Instruments. The ICP parameters were optimized using 80-sccm Ar flow rate, 80-mtorr chamber pressure, 480-w RF power, 500-w ICP power, 20°C temperature, 1-min time. After Ar plasma exposure, the samples were annealed at 600°C-800°C for 2 min in a rapid thermal processer (RTP) in a nitrogen atmosphere. Two fresh pieces of InP were used to provide an phosphorous over-pressure environment during the annealing process and further to prevent the sample surface from phosphorous outdiffusion. Room-temperature (RT) Photoluminescence (PL) measurements were then performed to obtain the bandgap energy shifts data.

Figure 3 shows the bandgap blue shift and PL peak intensity in different RTA temperature. Large bandgap shift of $\tilde{9}$0nm is obtained under RTA temperature of 750°C, while the PL peak

TABLE III
THE LAYER STRUCTURE FOR THE 0.9% COMPRESSIVE STRAIN INGAASP/INGAASP MULTIPLE QUANTUM WELL

Layer	Composition	Thickness(nm)	Doping(cm^{-3})
Sacrificial	InP	500	Zn
Cap	p^+-InGaAs	200	Zn:1e19
Cladding	p-InP	1500	Zn:1e18
Etch-stop	p-InGaAsP (1.24um)	10	Zn:4e17
Cladding	p-InP	150	Zn:4e17
GRINSCH	p-InGaAsP (1.05um)	20	Zn:4e17
GRINSCH	p-InGaAsP (1.15um)	20	Zn:4e17
GRINSCH	p-InGaAsP (1.24um)	20	Zn:4e17
QW	InGaAsP	5	–
Barrier×7	InGaAsP (1.24um)	10	–
QW×7	InGaAsP	5	–
GRINSCH	p-InGaAsP (1.24um)	20	Si:4e17
GRINSCH	p-InGaAsP (1.15um)	20	Si:4e17
GRINSCH	p-InGaAsP (1.05um)	20	Si:4e17
Buffer	n-InP	1500	Si:2e18
Substrate	n^+-InP	–	S or Sn: 4e18

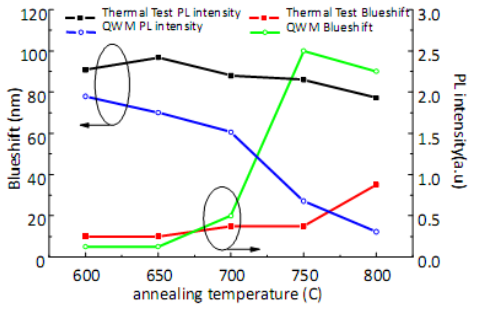

Fig. 3. Bandgap blue shift and PL peak intensity vs. RTA temperature

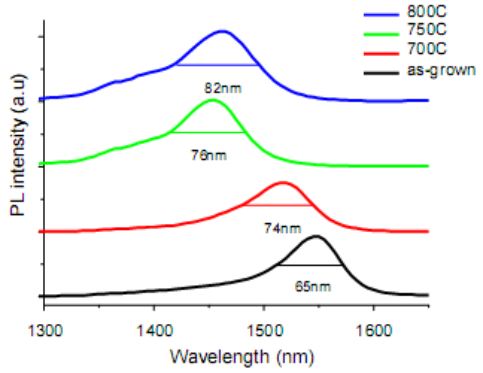

Fig. 4. PL vs. wavelength

intensity decrease of 80% is slight and acceptable.

Figure 4 shows the full width at half maximum (FWHM) of the PL under different RTA temperature. The slight linewidth broadening may result from different bandgap blue shift of TE and TM modes of the PL.

B. Waveguiding Characteristics

Subsection goes here.

In order to investigate the effect of argon plasma on waveguide quality, waveguide loss measurement using the Fabry-Perot fringe technique were performed. 3-μm-wide ridge waveguides were fabricated on the intermixed region. The sample was then cleaved to form a 1-mm-long Fabry-Perot cavity. A tunable (1.45-1.59μm) laser diode was used for the absorption experiments. The light was modulated at 10KHz and coupled into the TE mode of the waveguide through a tapered polarization preserving fiber. The transmitted light was then captured by a similar fiber coupled to a Ge-detector followed by a lock-in amplifier.

Figure 5 shows the measured transmitted spectra of the blue-shift waveguide cavity. Fabry-Perot interference fringes were formed due to multiple reflections at the cleaved facets. From the contrast of these fringe the waveguide loss can be determined by Equation 15,

$$L = 10\lg\left[\frac{1}{\sqrt{R_1 R_2}}\frac{1}{K_m}(1-\sqrt{1-K_m^2})\right] \qquad (15)$$

where R_1 and R_2 are the reflectivity of the cleaved facets and K_m is the contrast of the fringes.

Figure 6 presents the absorption as a function of wavelength derived from Figure 5 and Equation 15.

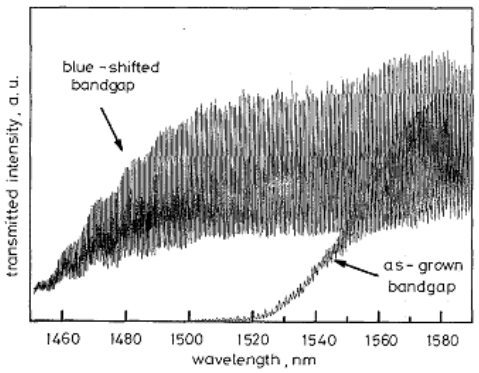

Fig. 5. Measured transmission spectra of blue-shifted waveguide

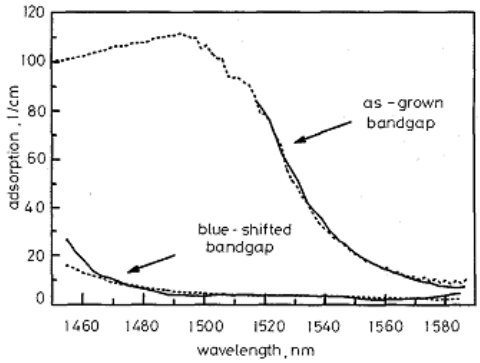

Fig. 6. Absorption constants derived from measured transmission spectra using modulation ratio and average transmission intensity for blue-shifted waveguide

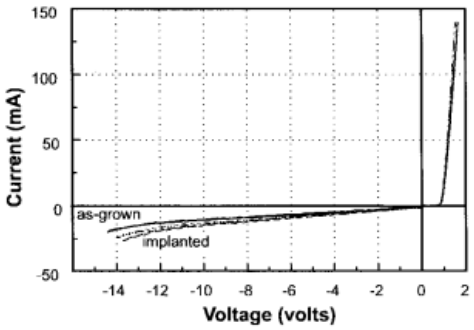

Fig. 7. I-V characteristics of p-i-n diodes made from as-grown and blue-shift materials

C. Electrical Characteristics

For the Ar plasma-induced QWI process to be a useful technique for lateral bandgap control in monolithic integration, it is essential that the electrical characteristics of the p-i-n structure not be degraded by the Ar plasma and/or anneal. Figure llll shows the current versus voltage (I-V) characteristics for the as-grown and blue-shift materials following a 120-s RTA at 750 °C. We see that all samples have very similar I-V characteristics.

D. Carrier Induced Tuning Characteristics

tuning? is vital!

IV. Application of QWI

A. Bandgap tuning of InP-Based Lasers

B. Extended Cavity Laser

V. Conclusion

The conclusion[11] goes here[12].

References

[1] John H. Marsh, "Quantum well Intermixing" *Semlcond. Sci. Technol*, vol.8, pp.1136-1155, 1993.

[2] Sylvain Charbonneau, Emil S. Koteles, P. J. Poole, J. J. He, G. C. Aers, J. Haysom, M. Buchanan, Y. Feng, A. Delage, F. Yang, M. Davies, R. D. Goldberg, P. G. Piva, and I. V. Mitchell, "Photonic Integrated Circuits Fabricated Using Ion Implantation" *IEEE JOURNAL OF SELECTED TOPICS IN QUANTUM ELECTRONICS*, vol.4, no.4, pp.772-793, 1998.

[3] B. S. Ooi, K. McIlvaney, M. W. Street, A. S. Helmy, S. G. Ayling, A. C. Bryce, J. H. Marsh, and J. S. Roberts, "Selective quantum-well intermixing in GaAsCAlGaAs structures using impurity-free vacancy diffusion" *IEEE J. Quantum Electron*, vol. 33, no. 10, pp. 1784C1793, Oct. 1997.

[4] S. P. McDougall, O. P. Kowalski, C. J. Hamilton, F. Camacho, B. Qiu, M. Kee, R. M. De La Rue, A. C. Bryce, and J. H. Marsh, "Monolithic integration via a universal damage enhanced quantum well intermixing technique" *IEEE J. Sel. Topics Quantum Electron*, vol. 4, no. 4, pp. 636C646, Jul./Aug. 1998.

[5] B. S.Ooi, T.K.Ong, andO.Gunawan, "Multiple-wavelength integration in InGaAsCInGaAsP structures using pulsed laser irradiation induced quantum well intermixing" *IEEE J. Quantum Electron.*, vol. 40, no. 5, pp. 481C490, May 2004.

[6] H. S. Djie, T. Mei, J. Arokiaraj, C. Sookdhis, S. F. Yu, L. K. Ang, and X. H. Tang, "Experimental and Theoretical Analysis of Argon Plasma-Enhanced Quantum-Well Intermixing" *IEEE JOURNAL OF QUANTUM ELECTRONICS*, VOL. 40, NO. 2, pp.166-174, Feb. 2004

[7] James W. Raring and Larry A. Coldren, "40-Gb/s Widely Tunable Transceivers" *IEEE JOURNAL OF SELECTED TOPICS IN QUANTUM ELECTRONICS*, vol.13, no.1, pp.3-14, 2007.

[8] *IEE Proc.-Optoelectron*, vol.149, no.4, August, 2002.

[9] D. Nie, T. Mei, X. H. Tang *et al* "Argon plasma exposure enhanced intermixing in an undoped InGaAsP/InP quantum-well structure" *J. Applied Physics*, 100, 046103, 2006

[10] D. Leong, H. S. Djie and P. Dowd, "A New Quantum Well Intermixing Technique Using Inductively Coupled Argon Plas ma on InGaAs/InGaAsP laser structures"

[11] H. Kopka and P. W. Daly, *A Guide to LaTeX*, 3rd ed. Harlow, England: Addison-Wesley, 1999.

[12] Banerjee M, Pal S. K. Roughness of fuzzy set. *Information Sciences*, 93:235∼246, 1996.

Xin Zhang was born in Zhejiang Province, China, in April 1986. He received the B.Eng. degree in information engineering from Zhejiang University, Zhejiang, China, in 2009. He is currently working toward the PhD degree in optical engineering at the same university. His current research interests are in the areas of design, optimization, and fabrication of photonic integrated circuits for optical communications systems.

Jian-Jun He received both the Diplome dEtudes Approfondies and Ph.D. degrees in semiconductor optoelectronics from the University of Paris VI, Paris, France, in 1986 and 1989, respectively. From 1986 to 1989, he worked at Center National dEtudes des Tlcommunications, Bagneux, France, on acoustooptical devices and the study of light scattering in semiconductor superlattices. He joined the Technical University of Nova Scotia, Halifax, NS, Canada, as a postdoctoral fellow in 1989 and later as a research associate, where he worked on semiconductor nonlinear optical devices. From 1994 to 2000, he was a Research Officer at the Institute for Microstructural Sciences, National Research Council of Canada, Ottawa, ON, Canada, working on semiconductor optoelectronic devices for dense-wavelength-division-multiplexing (DWDM) applications. From 2000 to 2002, he was with MetroPhotonics, Inc., where he was the founding Chief Scientist. He is now a specially appointed Changjiang Professor with the Department of Optical Engineering, Zhejiang University, and also a consultant with Lightip Technologies, Inc., Ottawa, ON, Canada. His current interest is multifunctional integrated optical components and subsystems for optical communications and biophotonics. He has published more than 100 scientific papers and holds fourteen US patents with a number of additional patents pending.